PROCEEDINGS OF SCIENCE

Implementation of the KM3NeT Online Core-Collapse Supernova neutrino search

C. Donzaud,[b] D. Dornic,[a,*] S. El Hedri,[b] I. Goos,[b] V. Kulikovskiy[c] and G. Vannoye[a,*] for the KM3NeT collaboration

[a] *Aix Marseille Univ, CNRS/IN2P3, CPPM, Marseille, France*
[b] *Université de Paris, CNRS, Astroparticule et Cosmologie, F-75013 Paris, France*
[c] *INFN, Sezione di Genova, Via Dodecaneso 33, Genova, 16146 Italy*

E-mail: dornic@cppm.in2p3.fr, vannoye@cppm.in2p3.fr

The detection of a neutrino burst from the next Galactic Core-Collapse Supernova (CCSN) will provide us invaluable information on this extreme phenomenon. Furthermore, the detection of its gravitational waves and electromagnetic signals would give us a complete picture of all emitted messengers. KM3NeT is a neutrino telescope consisting of two detectors, ORCA and ARCA, currently under deployment in the Mediterranean Sea. By looking for an excess of coincidence events above the optical background, it will be able to detect low-energy neutrinos from CCSN. A sensitivity to Galactic and near-Galactic events is expected when data from the two infrastructures is combined. With its integration in the SNEWS global alert network and the ongoing work to compute and combine the neutrino light-curves of different detectors, KM3NeT will play a key part in notifying other telescopes before the arrival of the other messengers. In this contribution, we present the real-time detection capabilities of KM3NeT, the additional information that can be brought by light-curve computations and the follow-up of external alerts.

38th International Cosmic Ray Conference (ICRC2023)
26 July - 3 August, 2023
Nagoya, Japan

*Speaker

PoS(ICRC2023)1223

1. Detection of CCSN neutrinos with KM3NeT

KM3NeT [1] is a distributed water Cherenkov neutrino telescope currently in construction in the Mediterranean sea. It is made of two detectors, ORCA offshore Toulon (France) at 2500 km depth and ARCA offshore Sicily (Italy) at 3500 km depth. Its detection principle is the reconstruction of neutrinos from the light induced from secondary interaction products using three dimensional arrays of photo-multipliers. The base component of these arrays is the Digital Optical Module (DOM) [12]: it is a pressure-resistant sphere containing 31 photo-multiplier tubes (PMTs) and embedded electronics to digitize the signal of the PMTs, as well as orientation sensors used to locate the DOM in real time. The DOMs are installed in groups of 18 in a vertical string called Detection Unit (DU) anchored to the seabed, with different spacing according to the detector. ORCA is more compact, optimized for the detection of tens of GeV neutrinos (mainly atmospheric neutrinos) and ARCA is a more voluminous, less dense detector, whose main goal is to discover astrophysical neutrino sources in the TeV to PeV energy range. KM3NeT is currently taking data with 16 DUs for ORCA and 21 DUs for ARCA and new DUs are continuously added to reach the objective of respectively 115 and 230 DUs by 2028.

Core-collapse supernovae are explosive phenomena ending the life of massive stars (above 10 solar masses) releasing a massive amount of energy (about 3×10^{53} erg) and causing a luminous stellar explosion. During the collapse, 99 % of the energy is released as low energy neutrinos (~ 10 MeV), emitted during a time window of a few hundreds of ms to one second. As the medium surrounding a proto-neutron star stays opaque to electromagnetic radiation for a few hours after the first emission of neutrinos, it is possible to detect those neutrinos on Earth before the CCSN becomes visible to light telescopes. This phenomenon allows for the possibility of alert systems: neutrino detectors could detect the neutrinos emitted during the core-collapse, eventually locating the source of those neutrinos, so that telescopes could observe all electromagnetic radiation emitted by a CCSN.

The main detection channel of KM3NeT for CCSN neutrinos is through inverse beta decay (IBD) of electron anti-neutrinos on free protons in the water ($\bar{\nu}_e + p \rightarrow e^+ + n$). As KM3NeT is optimized for the detection of neutrinos above the GeV scale, the individual positron trajectories cannot be reconstructed. Instead, the strategy adopted is to search for an excess of coincidences between PMTs in single DOMs above the expected background of the detector [2]. Apart from the PMT dark rate (about 1 kHz to 2 kHz) there are three main sources of optical background with KM3NeT: radioactive decay in the sea water (mostly ^{40}K), bioluminescence and atmospheric muons [10]. Radioactive decay causes a constant background in every PMT with a hit (PMT voltage rising above 0.3 photo-electrons) rate of about 7 kHz. Bioluminescence leads to a localized increase of the hit rates up to the MHz range, causing the need to veto rates above 20 kHz with the embedded electronics of the DOMs [11]. Finally, atmospheric muons generate long, downgoing tracks, inducing Cherenkov radiation detected by multiple DOMs, allowing to identify them.

In order to reject sources of optical background, a coincidence is defined as at least four hits within one DOM and with PMTs within 90 degrees of each other, with all the hits in a time window of 10 ns. The multiplicity of a given coincidence is the number of unique PMTs involved. Some of those coincidences are caused by atmospheric muons, but can be discarded using the muon reconstruction capabilities of the detector. The multiplicity distribution of the number of

coincidences due to optical background in 500 ms can be seen in Figure 1 left: in light blue markers for ORCA and dark blue markers for ARCA, shown for a fully built detector. On this plot, the number of coincidences that would be measured in the event of CCSN with progenitors of different masses at 10 kpc can be seen.

The optimal sensitivity is obtained for a multiplicity range between 6 and 10 and the coincidence level is defined as the number of coincidences in 500 ms within this multiplicity range. The right plot of Figure 1 shows the sensitivity of KM3NeT as a function of the distance of the CCSN. In the most conservative scenario (progenitor of mass 11 $M_\odot$), KM3NeT is able to observe 95 % of the Milky Way, and can go up to the Large Magellanic Cloud.

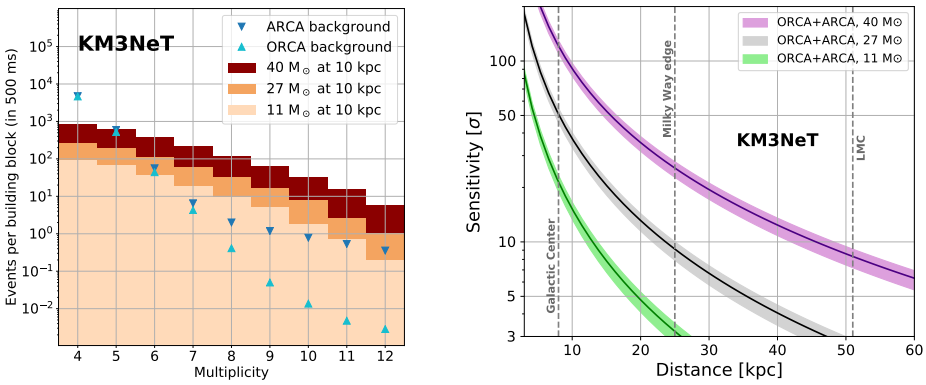

Figure 1: Left: expected number of events in a KM3NeT building block as a function of the multiplicity. The background is shown with markers in light blue for ORCA and dark blue for ARCA. The signal is represented with colored bars in orange shades for the different models: light for 11 $M_\odot$, intermediate for 27 $M_\odot$, dark for 40 $M_\odot$. Right: KM3NeT detection sensitivity as a function of the distance to the CCSN for the three progenitors considered: 11 $M_\odot$ (green), 27 $M_\odot$ (gray) and 40 $M_\odot$ (purple). The error bars include the systematic uncertainties. Figures from [2].

Those results describe the expected sensitivity with the analysis currently implemented within the current KM3NeT online system. Another method, which uses new observables to characterize the optical background, is also presented during this conference [3]. This new selection improves the overall sensitivity to a CCSN by $\sim$ 23 % and will be implemented in the online system before the end of 2023.

As the expected Galactic CCSN rate is 1.5 per century and the typical emission duration is a few hundred ms, a fast online system is needed to be ready for the next CCSN.

2. Description of the CCSN online pipeline

The CCSN online pipeline is part of the real-time multi-messenger analysis platform of KM3NeT [7], whose main goals are CCSN monitoring, which is presented in this contribution, searching for neutrinos correlated with external electromagnetic, gravitational waves (GW) or neutrinos alerts, which is presented in [8] and sending all-sky all-flavor neutrino alerts to external observatories for follow-up.

An overview of the CCSN online pipeline is given in Figure 2. It consists of multiple modules (small independent programs running on a common server to both detectors), which are organized

in three sections: the real-time CCSN search pipeline, in blue, analyzing the data collected by both KM3NeT detectors in order to evaluate a time-dependent significance that can be exploited to identify a CCSN signal and generate alerts; the quasi-online pipeline, in red, which is activated on special occasions to obtain and analyze data containing all detected coincidences, without selection on multiplicity or angle between PMTs; the triggered analysis pipeline, in yellow, made to follow-up external multi-messenger alerts in order to provide a fast response using a semi-automated analysis [6]. Those modules communicate through a common dispatcher, which is also running on the common server. The different networks connected to the pipeline to send or receive alerts and data are also represented in green.

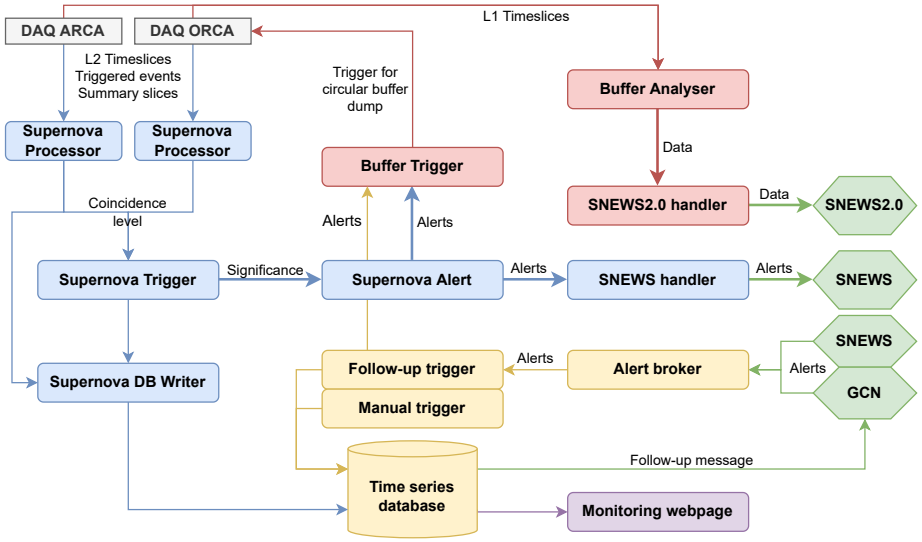

Figure 2: Scheme describing the dataflow of the CCSN online pipeline. The colors describe the three sections of the pipeline: in blue, the real-time CCSN search pipeline, to identify a CCSN signal and generate alerts; in red, the quasi-online pipeline, to extract parameters from all detected coincidences during an alert; in yellow, the triggered analysis pipeline, to follow-up external multi-messenger alerts.

The goal of the real-time CCSN search pipeline is to evaluate a time-dependent significance used to identify a CCSN and generate alerts that can be shared with networks such as SNEWS [4].

The first module of the chain is called Supernova Processor and computes every 100 ms the coincidence level. One Supernova Processor is running on each shore station, receiving low-level data in the form of timeslices (pack of segments of 100 ms of data) from the Data Acquisition (DAQ) system. As a reminder, the coincidence level is the number of coincidences between multiple PMTs with a maximal opening angle between them in single DOMs in a given time window length on which only coincidences with an optimal multiplicity are selected, before applying a veto to remove muon induced coincidences and finally summing the number of coincidences over 500 ms.

Coincidence levels from both detectors are sent to a common server, where the Supernova Trigger computes the combined Gaussian significance and the False Alarm Rate (FAR). The combined significance is obtained using a weighted linear combination of the ORCA and ARCA significance, where the weights are chosen as the detection sensitivity at a reference distance of 10 kpc for a benchmark flux model. In order to insure that the significance is computed correctly also in the case of an event during the downtime of one detector and to accommodate for the

variations of delay between the two detectors, the incoming data are queued for an configurable maximum amount of time, at the end of which the module computes the significance for only one detector. If data from the second detector arrive after this delay, they are stored for a potential triggered follow-up analysis, but are not considered in the real-time computation of the significance. A description of the method to compute the significance can be found in section 3.

The Supernova Alert module selects messages whose significance is above a threshold before triggering the last module, the SNEWS handler, which transmits the alert to the SNEWS network. Four thresholds are currently defined: `test`, alerts with an hourly FAR, used for internal monitoring purposes; `snews-low`, alerts with a FAR below one per day, sent as sub-threshold alerts; `snews`, alerts with a FAR below one every eight days, sent to SNEWS for alerting purposes; `high-Z`, alerts with a FAR below one per year, aimed at public advertising via the Gamma-ray Coordinates Network (GCN).

The quasi-online pipeline aims to retrieve all hits belonging to coincidences without selection in order to be able to perform further analyses based on the neutrino light-curve characterization, such as fit of the precise arrival time or detection of the standing accretion shock instability [2]. As this data cannot be stored continuously because of storage limitations, a circular buffer is implemented in the DAQ system to continuously cache 10 minutes of data. On request, a file containing the circular buffer is written on each shore station, and recovered to the common server. Currently, the events considered significant enough to trigger this writing are the following: `snews` alert sent by KM3NeT; reception of an external SNEWS alert; external gravitational wave observation of a compact binary merger involving at least one neutron star; GW detection of a significant burst event.

Once the data containing all coincidences have been written and retrieved using the Buffer Trigger module, the analysis is performed by the Buffer Analyzer module in order to build the neutrino light-curve and to fit it with given models. From this fit, the signal arrival time called T_0 is precisely determined, and transmitted along with the light-curve to the SNEWS2.0 network [5].

At the reception of an external alert, either through the GCN for the follow-up of GW or through the SNEWS system, the follow-up pipeline is automatically triggered. The principle of the search is to look for the maximum significance during a given time-window, which differs according to the type of alert: $[0, 2\,\mathrm{s}]$ for GW detection and $[-5\,\mathrm{s}, 5\,\mathrm{s}]$ for external CCSN alerts.

3. Adaptive background expectation

As written previously, bioluminescence in the sea may lead to a localized increase of the hit rates up to the MHz range per PMT, causing the need to veto rates above kHz within the embedded electronics of the DOMs. This leads to a non-constant number of active PMTs over the whole detector, which also causes variation in the expected background. This veto occurs more often with the ORCA detector due to the common bioluminescence in its location, thus the following text focuses on ORCA data.

If a constant expected background b and a coincidence level n for a given period of 500 ms is considered, computing the one sided p-value p, associated Gaussian significance zscore and daily FAR is straightforward using the following definition: $p = P_{\mathrm{Poisson}}(X \geq n; b)$, $p = \int_{\mathrm{zscore}}^{+\mathrm{inf}} P_{\mathrm{Gaussian}}(x)\,\mathrm{d}x$ and FAR [per day] $= 10 \times 86400 \times p$. The FAR is calculated as the product of the p-value and the update frequency of the search window, corresponding to $100\,\mathrm{ms}^{-1}$.

For a non-constant expected background, the relationship between b and the number of active PMTs needs to be properly established. Two previous determinations of the expected background as a function of the number of active PMTs have been done in the past, respectively for ORCA4 and ORCA6 [6, 9]. The first one, shown in Figure 3 left, considers a variable called "instrumentation efficiency", defined as the ratio between the expected background measured with a given fraction of active PMTs and the expected background measured with a fully active detector. The second one, which can be seen in Figure 3 right, considers directly the expected background (mean rate on the plot) as a function of active PMTs. For both plots, a binning is applied to the fraction of active PMTs and a linear relationship is found between expected background and number of active PMTs.

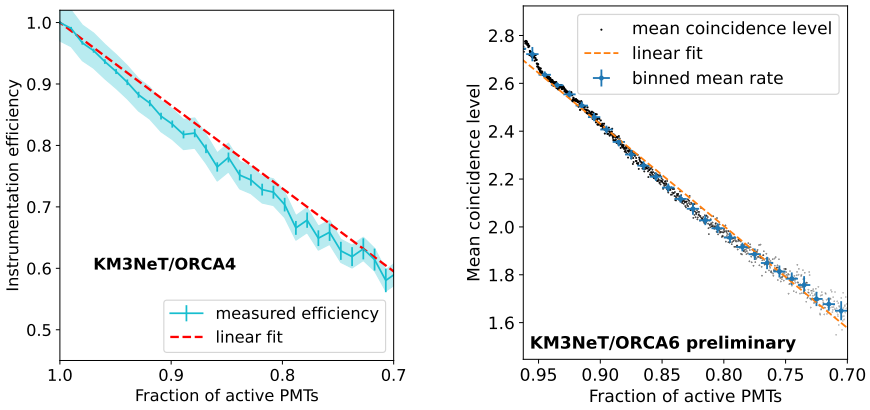

Figure 3: Left: Measured instrumentation efficiency as a function of the fraction of active PMTs in ORCA4 detector. The blue line shows the averaged measured efficiency with bins of width 0.01, monthly variability is covered by the shaded area and the dashed red line shows the linear fit applied to the date. Figure from [6]. Right: Mean rate of the coincidence level as a function of the fraction of active PMTs for ORCA6. Every black dot represents the computed mean rate averaged for the whole detector, for a given fraction of active PMTs. The blue crosses indicate averaged values in bins of width 0.05 and the orange dashed line is a linear fit of the binned data. Figure made to characterize the background for the MeV analysis of [9].

The issue with those two previous plots arises when drawing a scatter plot of values averaged over groups of ten minutes, as shown in the left of Figure 4, instead of applying a binning to the number of active PMTs. On this scatter plot, the mean number of active PMTs as a function of the mean expected background (*ie* coincidence level) is displayed, with the color representing the mean number of active DOMs during those 10 minutes. The relationship is no longer linear but seems to be quadratic, with multiple behaviors depending on the number of active DOMs.

The behavior seen in the left plot of Figure 4 can be easily explained by the fact that the detector with all lines and half of the PMTs active does not behave the same way as the detector with half of the lines and all PMTs active. The solution is to normalize both the coincidence level and the number of active PMTs by the number of active DOMs, as done in the right plot of Figure 4. On this figure, it can be seen that the detector follows a single quadratic function. A non-negligible variability is however still visible and needs to be taken into account. The goal of the following analysis is to show that a new quadratic fit needs to be performed frequently to factor in this variability and to insure a good estimation of the significance.

Data from the beginning of ORCA10 (December 2021) to ORCA18 (middle of June 2023) were processed using two different methods. In the first method, a single fit is performed with the

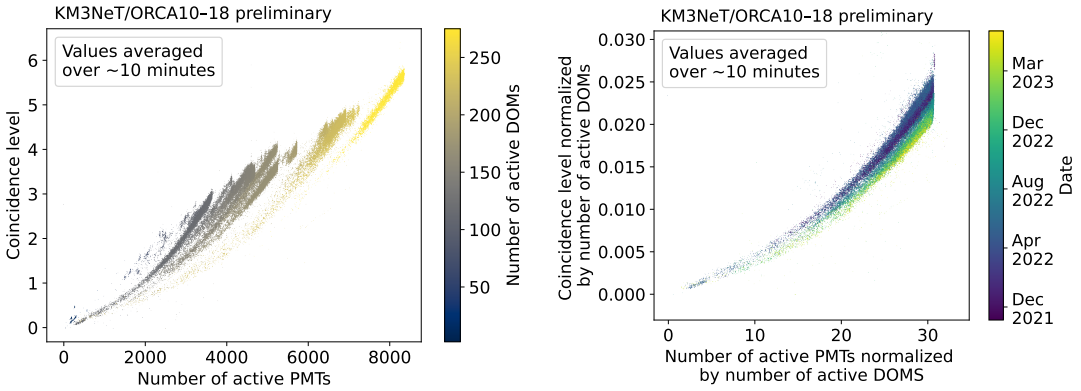

Figure 4: Left: Scatter plot of average over groups of 10 minutes of coincidence level vs number of active PMTs. The colors represent the average number of active DOMs during the 10 minutes period. Right: Scatter plot of average over groups of 10 minutes of coincidence level vs number of active PMTs both normalized by number of active DOMs. Time of the 10 minutes group is shown as a color. Both plots are made with data from ORCA10 to ORCA18.

first 30 days of data. For every timeslice, the expected background is computed from the fit, which is used to compute a zscore and an expected zscore distribution. In the second method, multiple fits are performed on groups of 30 days of data, and the expected background for a given timeslice is computed from the fit of the previous group. The choice of the 30-day period is a good compromise between the need to have enough data to be able to have a variation in the number of active PMTs to perform the fit and the need for the most recent behavior of the detector to be taken into account. The two distributions are computed in the same way as in the first method.

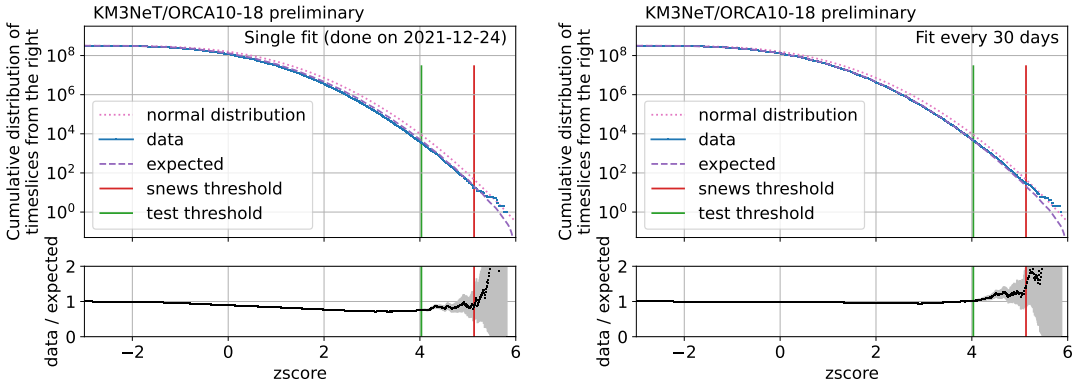

Figure 5: Cumulative distribution of timeslices from the right as a function of zscore computed for data from ORCA10 to ORCA18. The distribution of a normal variable is drawn in a dotted pink line; the expected number of timeslices in a purple dashed line; the number of timeslices obtained from data in a full blue line. Two threshold levels, `snews` (1 per 8 days) in red and `test` (1 per hour) in green are displayed for reference. A comparison between data and expected number of timeslices is also shown at the bottom. Left: distribution for a single fit (done from the first 30 days of data). Right: distribution for fits performed every 30 days.

The cumulative distributions from high zscore to low zscore for both methods are displayed on Figure 5 (left for single fit, right for multiple fits). This distribution gives the number of alerts

that would be sent for a given zscore threshold. A good agreement between the zscore distribution obtained from data (full blue line) and the expected zscore distribution (dashed purple line) would show that the expected background is properly estimated. The bottom plots of Figure 5 showing the relative comparison between them clearly indicate that for zscore below 4, the agreement between data and expected is much better using the second method. For zscore above 4, the statistical uncertainty starts to be predominant.

4. Conclusions

The CCSN online pipeline of KM3NeT is currently running with data from ORCA18 and ARCA21. The real-time CCSN search pipeline, looking for an excess of coincidences above the optical background, will be able to detect the next Galactic CCSN with a 5σ discovery potential. With the quasi-online pipeline, it is possible to perform further studies from the neutrino light-curve, such as the fit of the time of arrival of the neutrino burst. The triggered follow-up analysis can provide fast response to external alerts, whether from GCN or the SNEWS network. Finally, an improved estimation method for the expected background was also presented.

References

[1] S. Adrián-Martínez et al. (KM3NeT Collab.), *Letter of Intent for KM3NeT 2.0*, *J. Phys. G: Nucl. Part. Phys.* **43** (2016) 084001.
[2] S. Aiello et al. (KM3NeT Collab.), *The KM3NeT Potential for the next Core-Collapse Supernova Observation with Neutrinos*, *Eur. Phys. J. C* **81** (2021) 445.
[3] I. Goos et al. (KM3NeT Collab.), *Searching for Core-Collapse Supernova neutrinos at KM3NeT*, *PoS* (ICRC2023) 1160.
[4] P. Antonioli et al., *SNEWS: the SuperNova Early Warning System*, *New J. Phys.* **6** (2004) 114.
[5] S. Al Kharusi et al., *SNEWS 2.0: a next-generation supernova early warning system for multi-messenger astronomy*, New J. Phys. **23** (2021) 031201.
[6] S. Aiello et al. (KM3NeT Collab.), *Implementation and first results of the KM3NeT real-time core-collapse supernova neutrino search*, *Eur. Phys. J. C* **82** (2022) 317.
[7] F. Huang et al. (KM3NeT Collab.), *Real-time multi-messenger analysis framework for KM3NeT*, *JINST* **16** (2021) C09034 [2107.13908].
[8] S. Celli et al. (KM3NeT Collab.), *The Real-Time Analysis Platform of KM3NeT and its first results*, *PoS* (ICRC2023) 1125.
[9] M. Lamoureux et al. (KM3NeT Collab.), *Follow-up of O3 gravitational wave events with neutrinos in ANTARES and KM3NeT telescopes*, *PoS* (ICRC2023) 1506.
[10] S. Adrián-Martínez et al. (KM3NeT collab.), *Deep sea tests of a prototype of the KM3NeT digital optical module*, *Eur. Phys. J. C* **74** (2014) 3056.
[11] S. Aiello et al. (KM3NeT Collab.), *KM3NeT front-end and readout electronics system: hardware, firmware, and software*, *J. Astron. Telesc. Instrum. Syst.* **5** (2019) 046001 [1907.06453].
[12] S. Aiello et al. (KM3NeT Collab.), *The KM3NeT multi-PMT optical module*, *JINST* **17** (2022) P07038.

Full Authors List: The KM3NeT Collaboration

S. Aiello[a], A. Albert[b,bd], S. Alves Garre[c], Z. Aly[d], A. Ambrosone[f,e], F. Ameli[g], M. Andre[h], E. Androutsou[i], M. Anguita[j], L. Aphecetche[k], M. Ardid[l], S. Ardid[l], H. Atmani[m], J. Aublin[n], L. Bailly-Salins[o], Z. Bardačová[q,p], B. Baret[n], A. Bariego-Quintana[c], S. Basegmez du Pree[r], Y. Becherini[n], M. Bendahman[m,n], F. Benfenati[t,s], M. Benhassi[u,e], D. M. Benoit[v], E. Berbee[r], V. Bertin[d], S. Biagi[w], M. Boettcher[x], D. Bonanno[w], J. Boumaaza[m], M. Bouta[y], M. Bouwhuis[r], C. Bozza[z,e], R. M. Bozza[f,e], H.Brânzaş[aa], F. Bretaudeau[k], R. Bruijn[ab,r], J. Brunner[d], R. Bruno[a], E. Buis[ac,r], R. Buompane[u,e], J. Busto[d], B. Caiffi[ad], D. Calvo[c], S. Campion[g,ae], A. Capone[g,ae], F. Carenini[t,s], V. Carretero[c], T. Cartraud[n], P. Castaldi[af,s], V. Cecchini[c], S. Celli[g,ae], L. Cerisy[d], M. Chabab[ag], M. Chadolias[ah], A. Chen[ai], S. Cherubini[aj,w], T. Chiarusi[s], M. Circella[ak], R. Cocimano[w], J. A. B. Coelho[n], A. Coleiro[n], R. Coniglione[w] P. Coyle[d], A. Creusot[n], A. Cruz[al], G. Cuttone[w], R. Dallier[k], Y. Darras[ah], A. De Benedittis[e], B. De Martino[d], V. Decoene[k], R. Del Burgo[e], U. M. Di Cerbo[e], L. S. Di Mauro[w], I. Di Palma[g,ae], A. F. Díaz[j], C. Diaz[j], D. Diego-Tortosa[w], C. Distefano[w], A. Domi[ah], C. Donzaud[n], D. Dornic[d], M. Dörr[am], E. Drakopoulou[i], D. Drouhin[b,bd], R. Dvornický[q], T. Eberl[ah], E. Eckerová[q,p], A. Eddymaoui[m], T. van Eeden[r], M. Eff[n], D. van Eijk[r], I. El Bojaddaini[y], S. El Hedri[n], A. Enzenhöfer[d], G. Ferrara[w], M. D. Filipović[an], F. Filippini[t,s], D. Franciotti[w], L. A. Fusco[z,e], J. Gabriel[ao], S. Gagliardini[g], T. Gal[ah], J. García Méndez[l], A. Garcia Soto[c], C. Gatius Oliver[r], N. Geißelbrecht[ah], H. Ghaddari[y], L. Gialanella[e,u], B. K. Gibson[v], E. Giorgio[w], I. Goos[n], D. Goupilliere[o], S. R. Gozzini[c], R. Gracia[ah], K. Graf[ah], C. Guidi[ap,ad], B. Guillon[o], M. Gutiérrez[aq], H. van Haren[ar], A. Heijboer[r], A. Hekalo[am], L. Hennig[ah], J. J. Hernández-Rey[c], F. Huang[d], W. Idrissi Ibnsalih[e], G. Illuminati[s], C. W. James[al], M. de Jong[as,r], P. de Jong[ab,r], B. J. Jung[r], P. Kalaczyński[at,be], O. Kalekin[ah], U. F. Katz[ah], N. R. Khan Chowdhury[c], A. Khatun[q], G. Kistauri[av,au], C. Kopper[ah], A. Kouchner[aw,n], V. Kulikovskiy[ad], R. Kvatadze[av], M. Labalme[o], R. Lahmann[ah], G. Larosa[w], C. Lastoria[d], A. Lazo[c], S. Le Stum[d], G. Lehaut[o], E. Leonora[a], N. Lessing[c], G. Levi[t,s], M. Lindsey Clark[n], F. Longhitano[a], J. Majumdar[r], L. Malerba[ad], F. Mamedov[p], J. Mańczak[c], A. Manfreda[e], M. Marconi[ap,ad], A. Margiotta[t,s], A. Marinelli[e,f], C. Markou[i], L. Martin[k], J. A. Martínez-Mora[l], F. Marzaioli[u,e], M. Mastrodicasa[ae,g], S. Mastroianni[e], S. Miccichè[w], G. Miele[f,e], P. Migliozzi[e], E. Migneco[w], M. L. Mitsou[e], C. M. Mollo[e], L. Morales-Gallegos[u,e], C. Morley-Wong[al], A. Moussa[y], I. Mozun Mateo[ay,ax], R. Muller[r], M. R. Musone[e,u], M. Musumeci[w], L. Nauta[r], S. Navas[aq], A. Nayerhoda[ak], C. A. Nicolau[g], B. Nkosi[ai], B. Ó Fearraigh[ab,r], V. Oliviero[f,e], A. Orlando[w], E. Oukacha[n], D. Paesani[w], J. Palacios González[c], G. Papalashvili[au], V. Parisi[ap,ad], E.J. Pastor Gomez[c], A. M. Păun[aa], G. E. Păvălaş[aa], S. Peña Martínez[n], M. Perrin-Terrin[d], J. Perronnel[o], V. Pestel[ay], R. Pestes[n], P. Piattelli[w], C. Poirè[z,e], V. Popa[aa], T. Pradier[b], S. Pulvirenti[w], G. Quéméner[o], C. Quiroz[l], U. Rahaman[c], N. Randazzo[a], R. Randriatoamanana[k], S. Razzaque[az], I. C. Rea[e], D. Real[c], S. Reck[ah], G. Riccobene[w], J. Robinson[x], A. Romanov[ap,ad], A. Šaina[c], F. Salesa Greus[c], D. F. E. Samtleben[as,r], A. Sánchez Losa[c,ak], S. Sanfilippo[w], M. Sanguineti[ap,ad], C. Santonastaso[ba,e], D. Santonocito[w], P. Sapienza[w], J. Schnabel[ah], J. Schumann[ah], H. M. Schutte[x], J. Seneca[r], N. Sennan[y], B. Setter[ah], I. Sgura[ak], R. Shanidze[au], Y. Shitov[p], F. Šimkovic[q], A. Simonelli[e], A. Sinopoulou[a], M.V. Smirnov[ah], B. Spisso[e], M. Spurio[t,s], D. Stavropoulos[i], I. Štekl[p], M. Taiuti[ap,ad], Y. Tayalati[m], H. Tedjditi[ad], H. Thiersen[x], I. Tosta e Melo[a,aj], B. Trocmé[n], V. Tsourapis[i], E. Tzamariudaki[i], A. Vacheret[o], V. Valsecchi[w], V. Van Elewyck[aw,n], G. Vannoye[d], G. Vasileiadis[bb], F. Vazquez de Sola[r], C. Verilhac[n], A. Veutro[g,ae], S. Viola[w], D. Vivolo[u,e], J. Wilms[bc], E. de Wolf[ab,r], H. Yepes-Ramirez[l], G. Zarpapis[i], S. Zavatarelli[ad], A. Zegarelli[g,ae], D. Zito[w], J. D. Zornoza[c], J. Zúñiga[c], and N. Zywucka[x].

[a] INFN, Sezione di Catania, Via Santa Sofia 64, Catania, 95123 Italy
[b] Université de Strasbourg, CNRS, IPHC UMR 7178, F-67000 Strasbourg, France
[c] IFIC - Instituto de Física Corpuscular (CSIC - Universitat de València), c/Catedrático José Beltrán, 2, 46980 Paterna, Valencia, Spain
[d] Aix Marseille Univ, CNRS/IN2P3, CPPM, Marseille, France
[e] INFN, Sezione di Napoli, Complesso Universitario di Monte S. Angelo, Via Cintia ed. G, Napoli, 80126 Italy
[f] Università di Napoli "Federico II", Dip. Scienze Fisiche "E. Pancini", Complesso Universitario di Monte S. Angelo, Via Cintia ed. G, Napoli, 80126 Italy
[g] INFN, Sezione di Roma, Piazzale Aldo Moro 2, Roma, 00185 Italy
[h] Universitat Politècnica de Catalunya, Laboratori d'Aplicacions Bioacústiques, Centre Tecnològic de Vilanova i la Geltrú, Avda. Rambla Exposició, s/n, Vilanova i la Geltrú, 08800 Spain
[i] NCSR Demokritos, Institute of Nuclear and Particle Physics, Ag. Paraskevi Attikis, Athens, 15310 Greece
[j] University of Granada, Dept. of Computer Architecture and Technology/CITIC, 18071 Granada, Spain
[k] Subatech, IMT Atlantique, IN2P3-CNRS, Université de Nantes, 4 rue Alfred Kastler - La Chantrerie, Nantes, BP 20722 44307 France
[l] Universitat Politècnica de València, Instituto de Investigación para la Gestión Integrada de las Zonas Costeras, C/ Paranimf, 1, Gandia, 46730 Spain
[m] University Mohammed V in Rabat, Faculty of Sciences, 4 av. Ibn Battouta, B.P. 1014, R.P. 10000 Rabat, Morocco
[n] Université Paris Cité, CNRS, Astroparticule et Cosmologie, F-75013 Paris, France
[o] LPC CAEN, Normandie Univ, ENSICAEN, UNICAEN, CNRS/IN2P3, 6 boulevard Maréchal Juin, Caen, 14050 France
[p] Czech Technical University in Prague, Institute of Experimental and Applied Physics, Husova 240/5, Prague, 110 00 Czech Republic
[q] Comenius University in Bratislava, Department of Nuclear Physics and Biophysics, Mlynska dolina F1, Bratislava, 842 48 Slovak Republic
[r] Nikhef, National Institute for Subatomic Physics, PO Box 41882, Amsterdam, 1009 DB Netherlands
[s] INFN, Sezione di Bologna, v.le C. Berti-Pichat, 6/2, Bologna, 40127 Italy
[t] Università di Bologna, Dipartimento di Fisica e Astronomia, v.le C. Berti-Pichat, 6/2, Bologna, 40127 Italy
[u] Università degli Studi della Campania "Luigi Vanvitelli", Dipartimento di Matematica e Fisica, viale Lincoln 5, Caserta, 81100 Italy
[v] E. A. Milne Centre for Astrophysics, University of Hull, Hull, HU6 7RX, United Kingdom

[w] INFN, Laboratori Nazionali del Sud, Via S. Sofia 62, Catania, 95123 Italy
[x] North-West University, Centre for Space Research, Private Bag X6001, Potchefstroom, 2520 South Africa
[y] University Mohammed I, Faculty of Sciences, BV Mohammed VI, B.P. 717, R.P. 60000 Oujda, Morocco
[z] Università di Salerno e INFN Gruppo Collegato di Salerno, Dipartimento di Fisica, Via Giovanni Paolo II 132, Fisciano, 84084 Italy
[aa] ISS, Atomistilor 409, Măgurele, RO-077125 Romania
[ab] University of Amsterdam, Institute of Physics/IHEF, PO Box 94216, Amsterdam, 1090 GE Netherlands
[ac] TNO, Technical Sciences, PO Box 155, Delft, 2600 AD Netherlands
[ad] INFN, Sezione di Genova, Via Dodecaneso 33, Genova, 16146 Italy
[ae] Università La Sapienza, Dipartimento di Fisica, Piazzale Aldo Moro 2, Roma, 00185 Italy
[af] Università di Bologna, Dipartimento di Ingegneria dell'Energia Elettrica e dell'Informazione "Guglielmo Marconi", Via dell'Università 50, Cesena, 47521 Italia
[ag] Cadi Ayyad University, Physics Department, Faculty of Science Semlalia, Av. My Abdellah, P.O.B. 2390, Marrakech, 40000 Morocco
[ah] Friedrich-Alexander-Universität Erlangen-Nürnberg (FAU), Erlangen Centre for Astroparticle Physics, Nikolaus-Fiebiger-Straße 2, 91058 Erlangen, Germany
[ai] University of the Witwatersrand, School of Physics, Private Bag 3, Johannesburg, Wits 2050 South Africa
[aj] Università di Catania, Dipartimento di Fisica e Astronomia "Ettore Majorana", Via Santa Sofia 64, Catania, 95123 Italy
[ak] INFN, Sezione di Bari, via Orabona, 4, Bari, 70125 Italy
[al] International Centre for Radio Astronomy Research, Curtin University, Bentley, WA 6102, Australia
[am] University Würzburg, Emil-Fischer-Straße 31, Würzburg, 97074 Germany
[an] Western Sydney University, School of Computing, Engineering and Mathematics, Locked Bag 1797, Penrith, NSW 2751 Australia
[ao] IN2P3, LPC, Campus des Cézeaux 24, avenue des Landais BP 80026, Aubière Cedex, 63171 France
[ap] Università di Genova, Via Dodecaneso 33, Genova, 16146 Italy
[aq] University of Granada, Dpto. de Física Teórica y del Cosmos & C.A.F.P.E., 18071 Granada, Spain
[ar] NIOZ (Royal Netherlands Institute for Sea Research), PO Box 59, Den Burg, Texel, 1790 AB, the Netherlands
[as] Leiden University, Leiden Institute of Physics, PO Box 9504, Leiden, 2300 RA Netherlands
[at] National Centre for Nuclear Research, 02-093 Warsaw, Poland
[au] Tbilisi State University, Department of Physics, 3, Chavchavadze Ave., Tbilisi, 0179 Georgia
[av] The University of Georgia, Institute of Physics, Kostava str. 77, Tbilisi, 0171 Georgia
[aw] Institut Universitaire de France, 1 rue Descartes, Paris, 75005 France
[ax] IN2P3, 3, Rue Michel-Ange, Paris 16, 75794 France
[ay] LPC, Campus des Cézeaux 24, avenue des Landais BP 80026, Aubière Cedex, 63171 France
[az] University of Johannesburg, Department Physics, PO Box 524, Auckland Park, 2006 South Africa
[ba] Università degli Studi della Campania "Luigi Vanvitelli", CAPACITY, Laboratorio CIRCE - Dip. Di Matematica e Fisica - Viale Carlo III di Borbone 153, San Nicola La Strada, 81020 Italy
[bb] Laboratoire Univers et Particules de Montpellier, Place Eugène Bataillon - CC 72, Montpellier Cédex 05, 34095 France
[bc] Friedrich-Alexander-Universität Erlangen-Nürnberg (FAU), Remeis Sternwarte, Sternwartstraße 7, 96049 Bamberg, Germany
[bd] Université de Haute Alsace, rue des Frères Lumière, 68093 Mulhouse Cedex, France
[be] AstroCeNT, Nicolaus Copernicus Astronomical Center, Polish Academy of Sciences, Rektorska 4, Warsaw, 00-614 Poland

Acknowledgements

The authors acknowledge the financial support of the funding agencies: Agence Nationale de la Recherche (contract ANR-15-CE31-0020), Centre National de la Recherche Scientifique (CNRS), Commission Européenne (FEDER fund and Marie Curie Program), LabEx UnivEarthS (ANR-10-LABX-0023 and ANR-18-IDEX-0001), Paris Île-de-France Region, France; Shota Rustaveli National Science Foundation of Georgia (SRNSFG, FR-22-13708), Georgia; The General Secretariat of Research and Innovation (GSRI), Greece Istituto Nazionale di Fisica Nucleare (INFN), Ministero dell'Università e della Ricerca (MIUR), PRIN 2017 program (Grant NAT-NET 2017W4HA7S) Italy; Ministry of Higher Education, Scientific Research and Innovation, Morocco, and the Arab Fund for Economic and Social Development, Kuwait; Nederlandse organisatie voor Wetenschappelijk Onderzoek (NWO), the Netherlands; The National Science Centre, Poland (2021/41/N/ST2/01177); The grant "AstroCeNT: Particle Astrophysics Science and Technology Centre", carried out within the International Research Agendas programme of the Foundation for Polish Science financed by the European Union under the European Regional Development Fund; National Authority for Scientific Research (ANCS), Romania; Grants PID2021-124591NB-C41, -C42, -C43 funded by MCIN/AEI/ 10.13039/501100011033 and, as appropriate, by "ERDF A way of making Europe", by the "European Union" or by the "European Union NextGenerationEU/PRTR", Programa de Planes Complementarios I+D+I (refs. ASFAE/2022/023, ASFAE/2022/014), Programa Prometeo (PROMETEO/2020/019) and GenT (refs. CIDEGENT/2018/034, /2019/043, /2020/049. /2021/23) of the Generalitat Valenciana, Junta de Andalucía (ref. SOMM17/6104/UGR, P18-FR-5057), EU: MSC program (ref. 101025085), Programa María Zambrano (Spanish Ministry of Universities, funded by the European Union, NextGenerationEU), Spain; The European Union's Horizon 2020 Research and Innovation Programme (ChETEC-INFRA - Project no. 101008324).